



Study of ferromagnetic and ferroelectric properties of nanocrystalline $\text{Bi}_2\text{Mn}_4\text{O}_{10}$

Shereef A. Fareed¹ · Makram Ibrahim¹ · Ahmed E. Hannora² · M. M. El-Desoky³

Received: 25 August 2022 / Accepted: 12 October 2022 / Published online: 29 October 2022
© The Author(s) 2022

Abstract

Nano-crystalline bismuth manganese oxide $\text{Bi}_2\text{Mn}_4\text{O}_{10}$ was prepared from Bi_2O_3 and MnO_2 by mechanochemical technique at different milling times followed by heat treatment at 1073 K. The crystal structural were obtained using X-ray diffraction (XRD) and TEM. We obtained the variation of the crystallite size and micro-strain with milling time. The magnetic parameters include the saturation magnetization, coercivity and squareness ratio were obtained by vibrating sample magnetometer (VSM). Each of the coercive field, Squareness ratio and saturation magnetization increased with increasing the milling time. The electrical conduction of the prepared samples was evaluated by AC conductivity measurements at different temperature, the dielectric parameters were plotted against temperature at different frequencies. The conduction mechanism is described by the correlated barrier hopping model (CBH). The recoverable energy density and loss energy was obtained to calculate the storage energy efficiency.

Keywords Bismuth manganese oxide · Nano-structure · Mechanochemical technique · AC electrical conductivity · Magnetic properties

1 Introduction

As a part of a series of studies, we are concerned in the current work with the ferromagnetic, ferroelectric behavior and AC conductivity of a mechanical treated samples (mix of Bi_2O_3 and MnO_2) at different milling times followed by heat tenement at 1073 K. In a related published work [1], we investigate the DC conductivity and Seebeck coefficient of the same samples, Bismuth manganese oxide with the chemical formula $\text{Bi}_2\text{Mn}_4\text{O}_{10}$ was described as a multiferroic material [2, 3]. In general, bismuth manganese oxides and perovskite are very promising because they mostly owned combinational properties lead to a wide

valuable applications [4–10]. A multiferroic material has ferroelectricity, ferromagnetism and/or ferroelasticity or generally, it has two or more ferroic polarization. Bismuth manganese oxides such as $\text{Bi}_2\text{Mn}_4\text{O}_{10}$ crystallizes in orthorhombic structure with space group (Pbam), the structure has two sites octahedral and pyramidal [11–13]. The coexistence of both ferromagnetic and ferroelectric properties attributed to the unpaired electrons and the orbital ordering of Manganese cations. There are different preparation methods for bismuth manganese oxides such as sol–gel combustion and high energy ball milling. The preparation of the constituent oxides in a ball milling technique required high energy and high pressure [14, 15]. For example, The perovskite formula $\text{Ba}_{0.85}\text{Ca}_{0.15}\text{Zr}_{0.1}\text{Ti}_{0.9}\text{O}_3$ formed in a single crystal starting from 8 h of milling time reaching to a complete homogeneous powder after 15 h. One of the important parameters is the variation of the dielectric constant with temperature, it was obtained at different frequencies [16]. This paper is reported to study the effect of mechanochemical preparation technique at different milling times followed by heat treatment at 1073 K on the structure, ferroelectric, ferromagnetic and dielectric properties of nanocrystalline $\text{Bi}_2\text{Mn}_4\text{O}_{10}$.

✉ Shereef A. Fareed
shereefscience@gmail.com

¹ Solar and Space Research Department, National Research Institute of Astronomy and Geophysics (NRIAG), Helwan 11421, Cairo, Egypt

² Department of Sciences and Engineering Mathematics, Faculty of Petroleum and Mining Engineering, Suez University, Suez 4351, Egypt

³ Department of Physics, Faculty of Science, Suez University, Suez 43518, Egypt

1.1 Experimental work

Source-materials from bismuth and manganese oxides ($\text{Bi}_2\text{O}_3/\text{MnO}_2$) with high purity 99% were prepared using the mechanochemical process, the oxides were mixed by a ball milling machine for different milling times followed by heat treatment at 1073 K. The structure was investigated at different milling times (1, 5, 10, 30 and 50 h) using X-ray diffraction and High resolution magnified images of the transmission electron microscope using the “SIEMENS D5000” X-ray diffractometer with target $\text{CuK}\alpha$ radiation and the “JEOL 2100 HRT” HRTEM respectively. A portion of each sample was pressed using a uniaxial hydraulic press to form pellets with 10 mm diameter under applying pressure of five tons. The magnetic parameters were obtained using the vibrating sample magnetometer (VSM) at room temperature using the “Lake shore 7410” VSM.

A computerized LCR meter bridge up to 1 MHz was connected with electrical-controlled furnace to measure the temperature-dependent AC electrical parameters. Sawyer–Tower circuit was used to obtain the electrical hysteresis loop of one of the prepared samples to assure the value of the ferroelectric/paraelectric transition temperature as obtained from dielectric measurements.

2 Results and discussion

2.1 Structure

Figure 1(a) shows the XRD patterns of mechanically treated samples, it's clear that the broadening increased with increasing the milling time reaching to an amorphous state. The effect of heat treatment on the mechanically prepared samples at 1037 K and different times is shown in Fig. 1b. According to The ICDD card “01-074-1096”, bismuth manganese oxide phase with chemical formulas $\text{Bi}_2\text{Mn}_4\text{O}_{10}$ was formed after 5 h of milling time followed by heat treatment at 1073 K. The phase $\text{Bi}_2\text{Mn}_4\text{O}_{10}$ formed in orthorhombic crystal structure and space group Pbam. The samples at 30 and 50 h showed a small amount of tetragonal Mn_3O_4 phase with space group I41/amd, the orthorhombic phase $\text{Bi}_2\text{Mn}_4\text{O}_{10}$ decreased after 10 h of milling time and it decomposes to $\alpha\text{-Bi}_2\text{O}_3$ and $\alpha\text{-Mn}_2\text{O}_3$. The ICDD card 03-065-2776 represents a few amount of Mn_3O_4 with tetragonal structure and space group I41/amd while the card 01-081-0563 represents the spectrum of bismuth oxide $\text{Bi}_{12.8}\text{O}_{12}$ with tetragonal system and space group I41/amd.

Figure 2 shows different formation percentages of the phases $\text{Bi}_2\text{Mn}_4\text{O}_{10}$, Mn_3O_4 and $\text{Bi}_{12.8}\text{O}_{19.2}$ at each milling time. 88% of the phase $\text{Bi}_2\text{Mn}_4\text{O}_{10}$ is formed with the

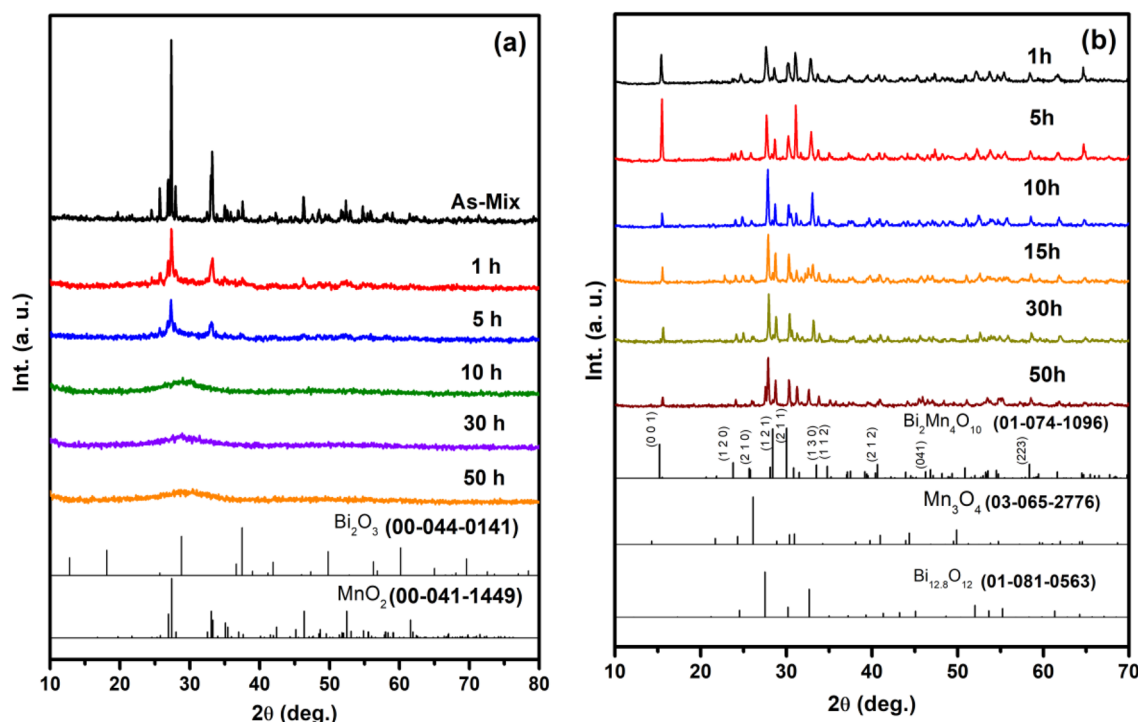


Fig. 1 XRD patterns of **a** mechanical treatment of the mixed oxides $\text{Bi}_2\text{O}_3/\text{MnO}_2$ without heat treatment, **b** samples after heat treatment at 1037 K

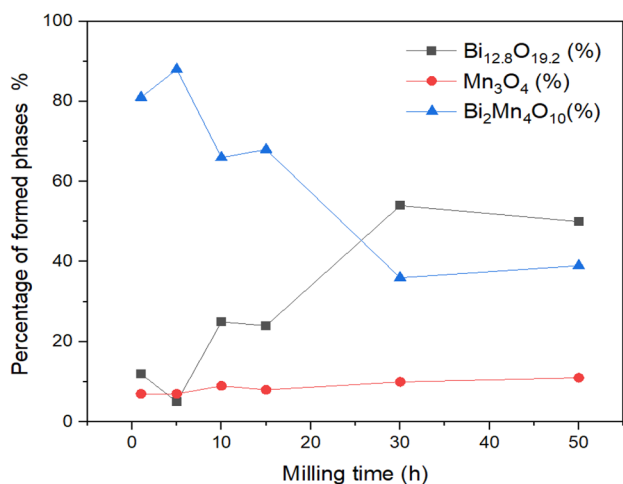


Fig. 2 Percentages of the formed phases with milling time

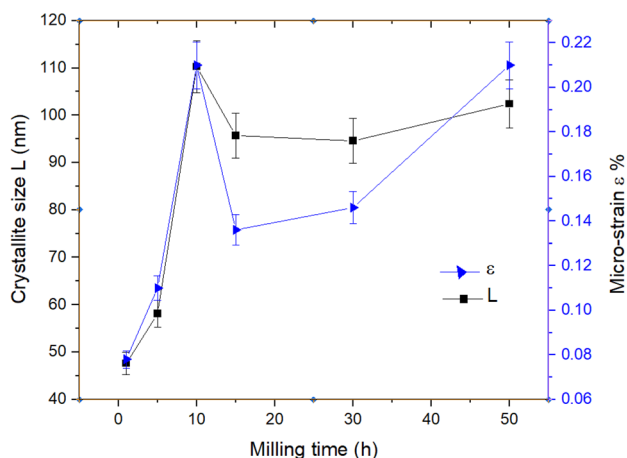


Fig. 3 Variation of crystallite size and micro-strain of heat-treated samples against milling time in hours

smallest percentages of the other oxides (5% of $\text{Bi}_{12.8}\text{O}_{19.2}$ and 7% of Mn_3O_4) at the milling time 5 h. Such a method in Fig. 2 has appeared in many published studies [17, 18]. The crystallite size varied from 47.6 to 110 nm, the variation of micro-strain and crystallite size against milling time is illustrated in Fig. 3. The orthorhombic structure of $\text{Bi}_2\text{Mn}_4\text{O}_{10}$ has (001) preferred orientation after 1 and 5 h of heat treatment. The octahedral-coordinated Mn^{4+} cations and Mn^{3+} cations are located in square pyramids. The cation distribution and oxygen stoichiometry are considered as the origin of the relatively phase difference at each milling time as well as the changes in the unit cell volume and concentration of manganese cations “N”, so the exchange interaction and the resultant magnetic and electric properties will be influenced. The effect of oxygen

stoichiometry of some manganites on the magnetic and electric properties is reported in many studies [1].

The full-width at half maximum (β) is obtained from the highest peaks to calculate the crystallite size (L) of each sample using Hall–Williamson as given in Eq. (1) [19]:

$$\beta \cos \theta = \frac{k\lambda}{L} \quad (1)$$

where λ is the wavelength, k is the Scherrer constant (shape factor) and (θ) is the Bragg angle, β represent the full width at half maximum of the highest peak which obtained using “Origin” software. As shown in Fig. 3, the micro-strains was estimated from the Hall-Williamson relation, it is varied from 0.078 to 0.210 (%). The micro-strain generated in the samples is related to their reaction during mechanical treatment, this enhanced the destabilization of the crystal structure.

Figure 4 shows The TEM images of the prepared samples (heated at 1073 K) at different milling time of 5, 10 and 50 h, the graphs show the multigrain structure at 50 nm magnification scale clarifying the d-spacing, it was 2.7 Å for the sample milled at 5 h, 2.4 Å for the sample milled at 10 h and 2.9 Å for the sample milled at 50 h. this agreed well with the corresponding d values from XRD spectrum data. Figure 5 shows their diffraction patterns, spots and concentric circles confirmed the poly crystalline structure of the prepared samples. The main phase planes are labeled at the sample of 5 h of milling time.

As appeared from the TEM graphs, the sample (a) owned the lower polycrystallinity compared with the samples milled at 10 and 50 h. From XRD, the obtained average crystallite size for the samples (a), (b) and (c) are 58, 108 and 101 nm respectively.

2.2 Magnetic properties

The magnetic behavior of the prepared samples was investigated by vibrating sample magnetometer. The obtained magnetic ordering is generated from the unpaired electrons of manganese cations [20]. As illustrated in Fig. 6 the magnetic hysteresis loop of the samples milled at 5, 10 and 50 h showed soft magnetic behavior at room temperature, the corresponding values of saturation magnetization (M_s), retentivity (M_r), Coercivity (H_c) and squareness ratio are listed in (Table 1). The sample at 5 h of milling time owned the minimum value of the coercive field (H_c) which is the required field to minimize the magnetization to its minimum value. The obtained values of squareness ratio confirmed the soft magnetic behavior of the three samples at room temperature, it's obvious that the softness decreased by increasing the milling time while each of the saturation magnetization (M_s), retentivity (M_r) and Coercivity (H_c) was increased

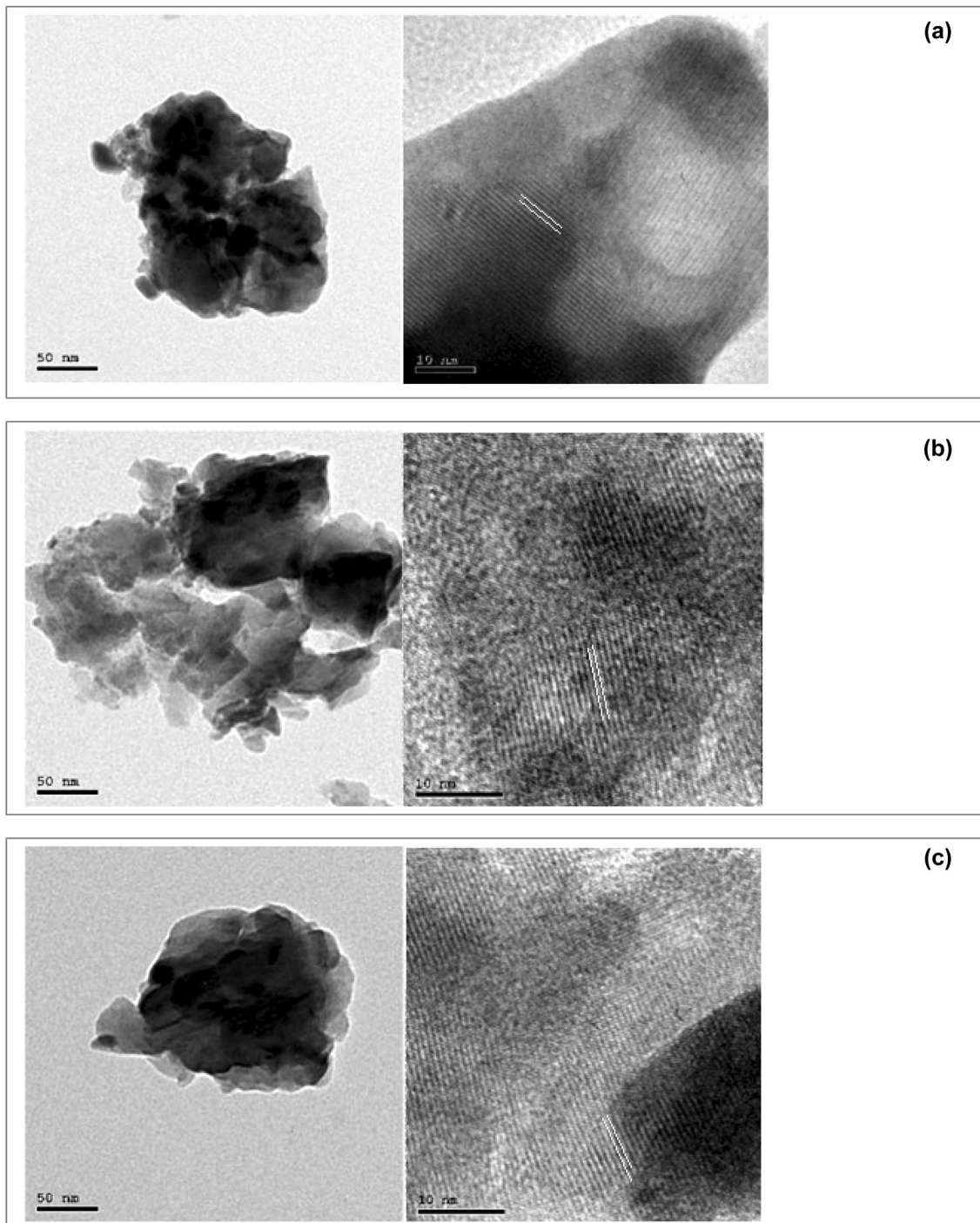


Fig. 4 TEM of the heat-treated samples (1073 K) milled at different milling time **a** 5 h, **b** 10 h and **c** 50 h

with increasing the milling time. According to the obtained data in (Table 1), the samples can be used in high frequency applications or high energy conversion transducers [21].

However, according to the above results it's recommended to obtain the magnetic behavior at low temperature, this is agreed with previous research work stated that, the Curie temperature lie approximately between 40

and 66 K for bismuth manganite [20, 22] which means that the ferromagnetic behavior take a place in lower temperature. As clearly obtained, the increasing in magnetic parameters with increasing the milling time is backed to structural distortion or different dopant ionic radii which reflect different percentages of the formed phases [23, 24].

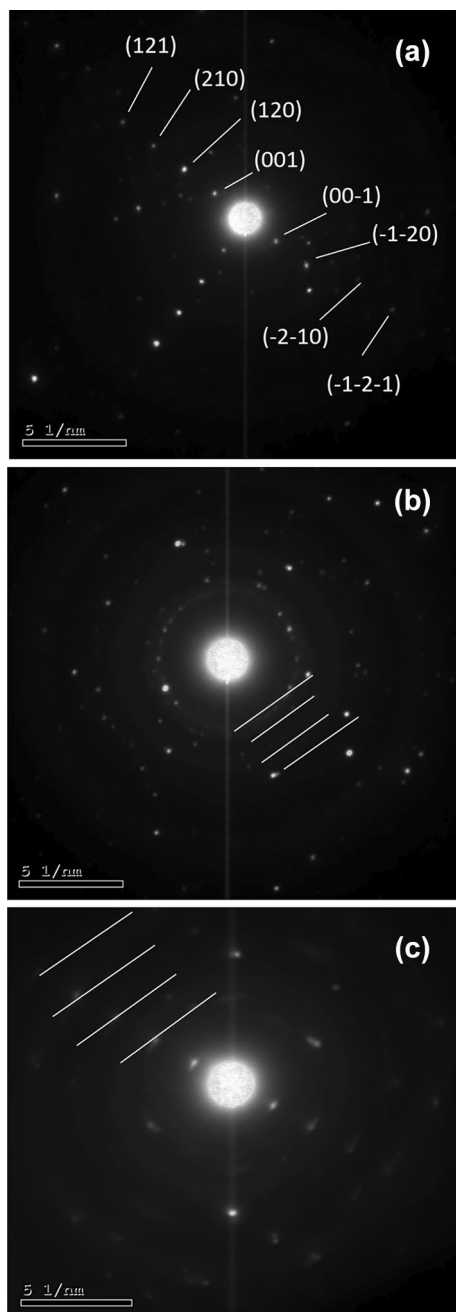


Fig. 5 TEM diffraction patterns of the heat-treated samples (1073 K) milled at different milling time **a** 5 h, **b** 10 h and **c** 50 h

2.3 Dielectric properties

It is known that, the electrical energy storage in dielectric materials is represented by the dielectric constant (ϵ') while the dissipated energy is denoted by ϵ'' , the variation of ϵ' , ϵ'' and $\tan \delta$ with temperature at different frequencies is obtained in Figs. 7, 8 and 9 for the heat-treated samples milled at 5, 10 and 50 h. The highest appeared peaks are due to the ferroelectric transition temperature (T_c) where

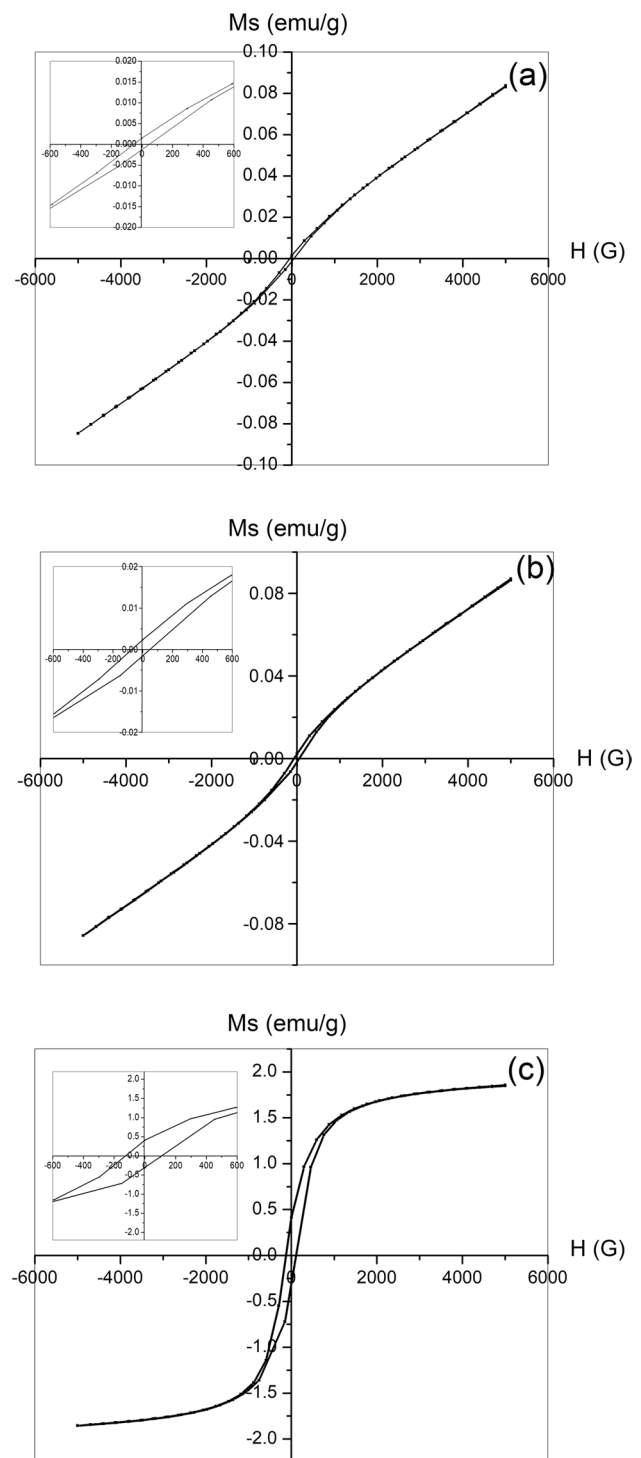


Fig. 6 VSM at room temperature for the heat-treated samples (1073 K) milled at different milling time **a** 5 h, **b** 10 h and **c** 50 h

the dipoles polarization lag behind the applied electric field, to assure that the values of T_c is really matched with ferroelectricity, we plot the electric hysteresis loop (Fig. 10) of the sample milled at 50 h, we noted that the loop is nearly disappeared at 453 K which is approximately the same

Table 1 Magnetic parameters of the sample milled for 50 h at room temperature

Milling time (h)	Squareness ratio	M_r (emu/g)	M_s (emu/g)	H_c (G)
5	0.014	0.00117	0.0842	41.157
10	0.021	0.00184	0.0864	55.277
50	0.194	0.35990	1.8552	119.67

temperature (456 K) at the highest peak. The other small peak is related to structural changes as reported previously [25]. It's obvious that the ferroelectricity transition temperature is decreasing with increasing the milling time. We evaluate the energy storage properties of the samples, Eqs. 2, 3 and 4 show how we can obtain the recoverable energy density (W_r), total energy density (W_t) and the energy storage efficiency (η) respectively. At room temperature (303 K), the value of W_r was 0.0496 mj/cm³ with energy loss $W(\text{loss})$ of 3.8895 mj/cm³ while at 453 K, W_r increased to 68.789 mj/cm³ and the energy loss decreased to be 0.99 mj/cm³.

$$W_r = \int_{P_r}^{P_{\max}} EdP \tag{2}$$

$$W_t = \int_0^{P_{\max}} EdP \tag{3}$$

$$\eta = \frac{W_r}{W_r + W(\text{loss})} \times 100 \tag{4}$$

where P_{\max} , E , P_r , and $W(\text{loss})$ are maximum polarization, applied electric field, remnant polarization, and energy loss density. The W_r , W_t and $W(\text{loss})$ are calculated by measuring the internal and external areas of the polarization versus electric field (P–E) curves. The energy storage efficiency (η) increased from 1.26% at 303 K to be 98% at 453 K.

The dielectric constant varied with milling time due to the different percentage of the formed phases which illustrated in Fig. 2, it's obvious that the sample after 5 h of milling time owned the maximum value of dielectric constant (approximately 20,000 at 100 Hz). The dissipation factor or loss tangent $\tan\delta$ is given from the ratio in Eq. 5.

$$\text{Tan}\delta = \frac{\epsilon'(\omega)}{\epsilon''(\omega)} \tag{5}$$

where $\omega = 2\pi f$. [21, 22]s

The temperature-dependence of loss tangent is shown in Fig. 9 its clear that $\tan \delta$ increases with increasing

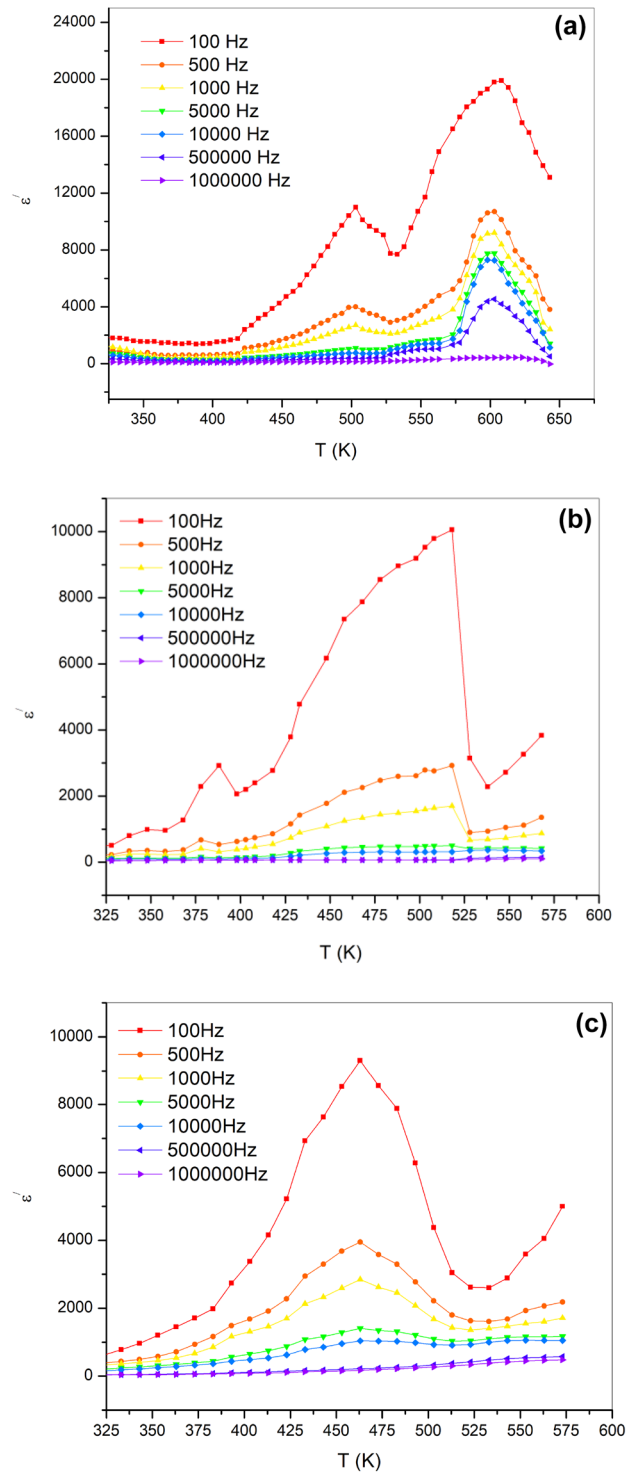


Fig. 7 Variation of ϵ'' with temperature at different frequencies for the heat-treated samples (1073 K) milled at different milling time **a** 5 h, **b** 10 h and **c** 50 h

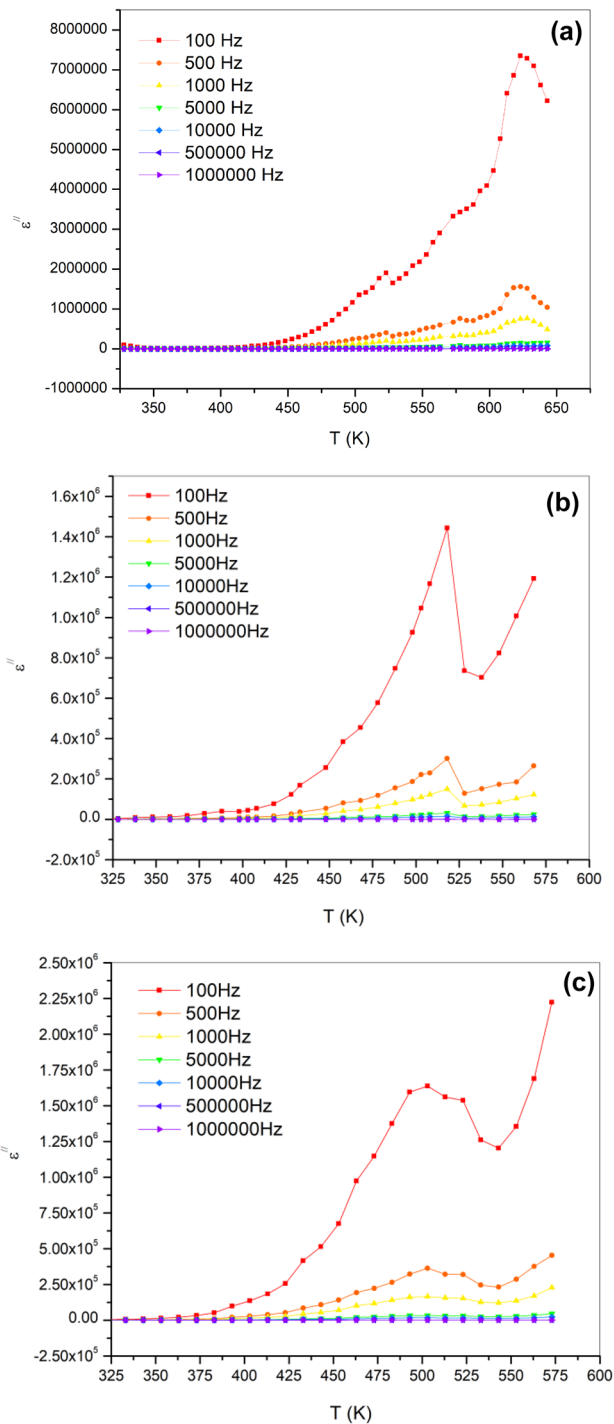


Fig. 8 Variation of ϵ'' with temperature at different frequencies for the heat-treated samples (1073 K) milled at different milling time **a** 5 h, **b** 10 h and **c** 50 h

temperature, this is due to the thermal activation of electrons, the observed peaks at low temperature is attributed to the electrons hopping frequency matching with frequency of applied electric field. At high temperature

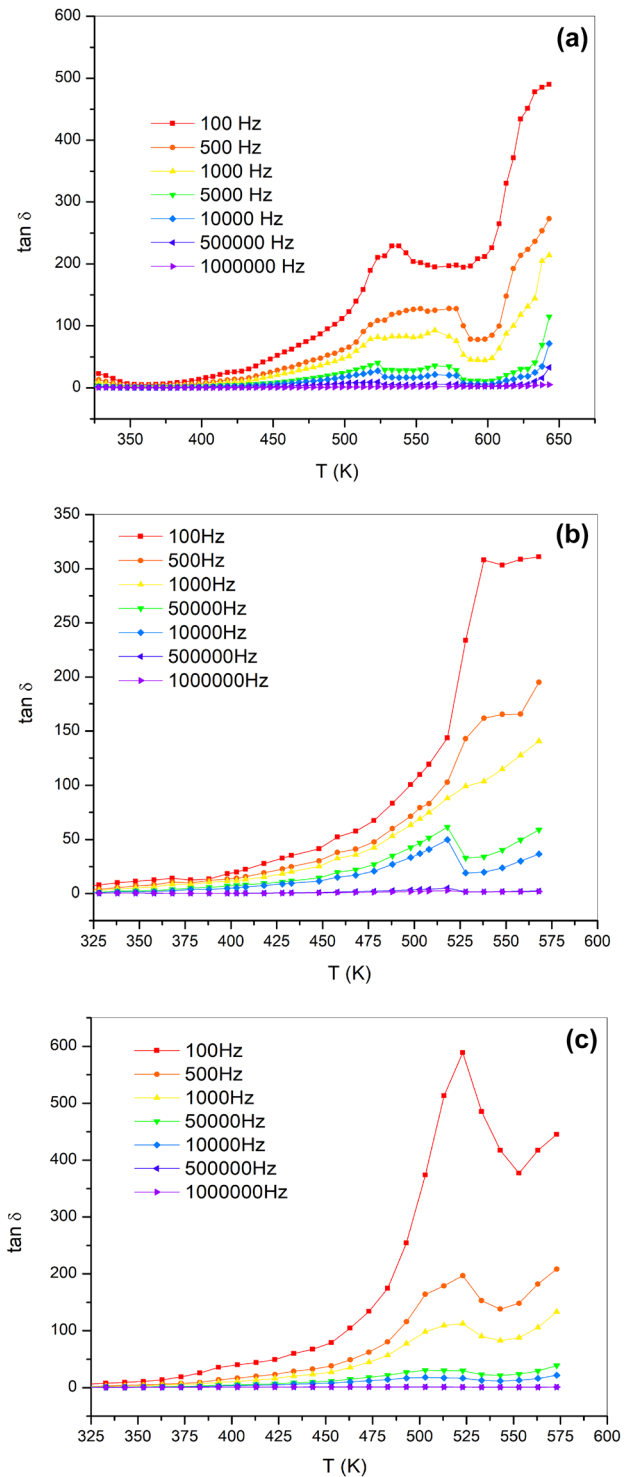


Fig. 9 Variation of $\tan \delta$ with temperature at different frequencies for the heat-treated samples (1073 K) milled at different milling time **a** 5 h, **b** 10 h and **c** 50 h

the relaxation is belong to the oxygen vacancies [24]. Figure 11 represents the frequency dependent electrical modulus where the semi-circular arcs of the real modulus

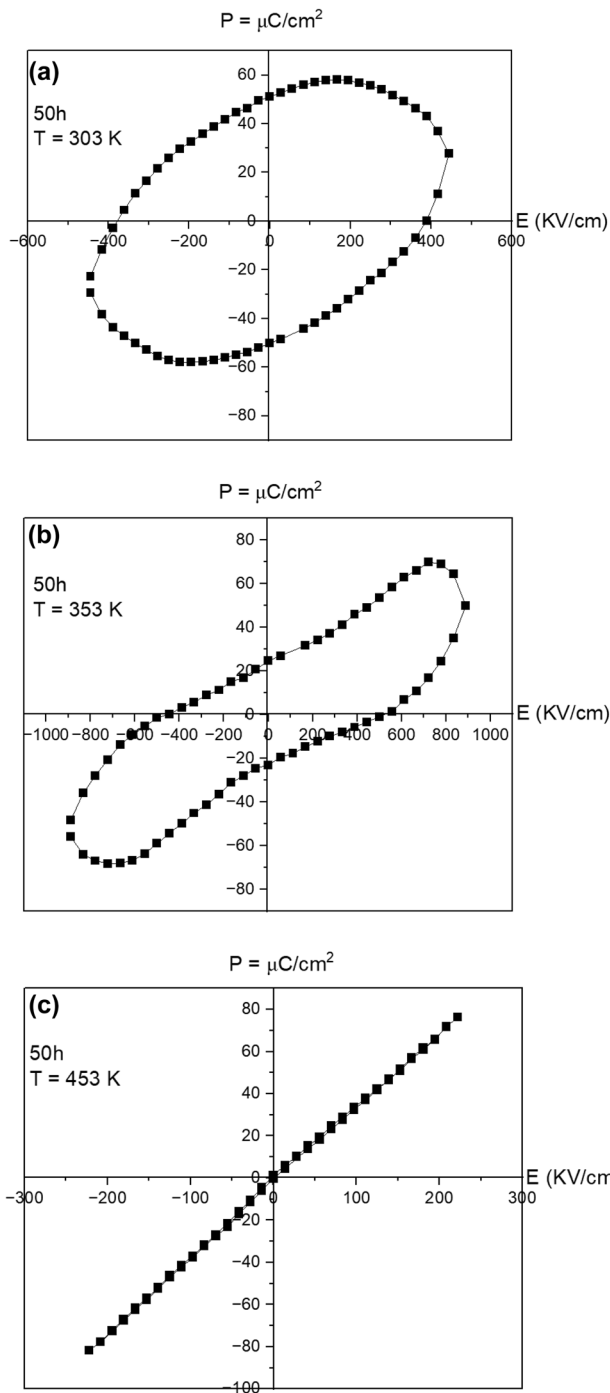


Fig. 10 ferroelectric hysteresis loops of the prepared sample (milled at 50 h) at different temperature **a** at 303 K, **b** at 353 K and **c** at 453 K

(M') versus the imaginary (M'') is plotted for the samples milled at 5, 10 and 50 h, the modulus M' and M'' are given by the following equations [26]:

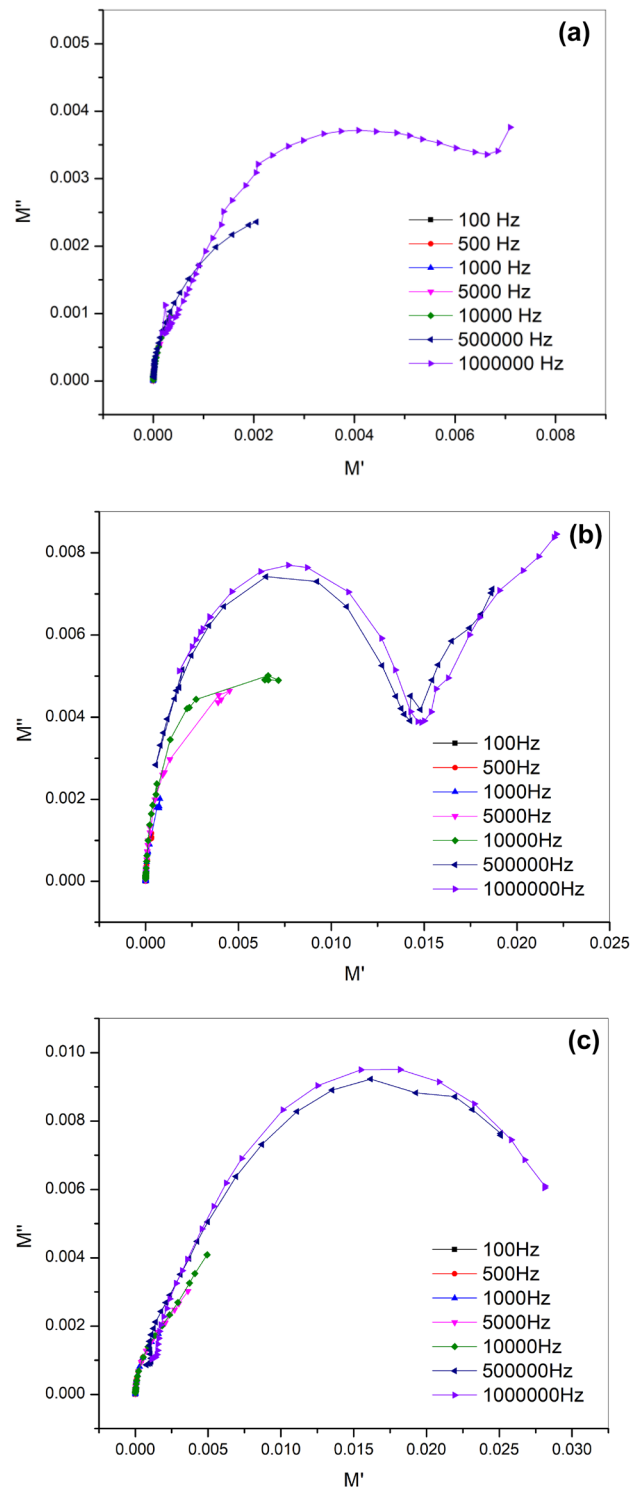


Fig. 11 Variation of M'' versus M' for the heat-treated samples (1073 K) milled at different milling time **a** 5 h, **b** 10 h and **c** 50 h

$$M' = \frac{\epsilon'}{\epsilon'^2 + \epsilon''^2} \tag{6}$$

$$M'' = \frac{\epsilon''}{\epsilon'^2 + \epsilon''^2} \quad (7)$$

The peaks are attributed to the short and long range hopping of charge carrier from an ionic state to neighboring ionic one.

As appeared from the Relaxation processes, At high frequency, the large semi-circular arcs represent the bulk or grain response while at low frequencies, the weak grain boundaries effect took a place [27]

Figure 12 shows the variation of logarithmic AC conductivity with $1000/T$ at different frequencies for the heat-treated samples (at 1073 K) milled at different time 5, 10 and 50 h.

The logarithmic a.c. conductivity increased with increasing temperature for all samples except the sample at 5 h of milling time where at low temperature it increased with temperature and then decreased gradually to its minimum value and redirected again to increased with the higher temperature degrees, at the first vertex point, the hopping of charge carrier is influenced by the applied frequency more than the thermal energy and inversely, at the second vertex, the thermal energy overcame the frequency effect.

The a.c. conductivity is related to the DC by Jonscher relation:

$$\sigma_{ac} = \sigma_{dc} + A\omega^s \quad (8)$$

where ω is the angular frequency. $A\omega^s$ represents the pure AC conductivity. A is constant, $A = \pi N^2 e^2 / 6 K_B T (2\alpha) N$ is the number of sites per unit volume among which hopping takes place. S is the frequency exponent, $0 \leq s \leq 1$.

The conductivity mechanism could be explained by the temperature-dependent behavior of (s), Several models were proposed in previous work [28–32], the exponent s can be calculated from the slope of $\ln \sigma$ versus $\ln \omega$ at different temperature as shown in Fig. 13, the temperature dependency of s values are obtained in Fig. 14. It's obvious that the exponent s decreased with increasing temperature, in this range the conduction mechanism can be described by the correlated barrier hopping (CBH).

3 Conclusion

The mechanochemical milling time is not linear parameter for preparing the phase $\text{Bi}_2\text{Mn}_4\text{O}_{10}$. According to the squareness ratio which is ranged from 0.014 to 0.194, all the prepared samples behave a soft magnetic ordering at room temperature. The sample milled at 5 h which is

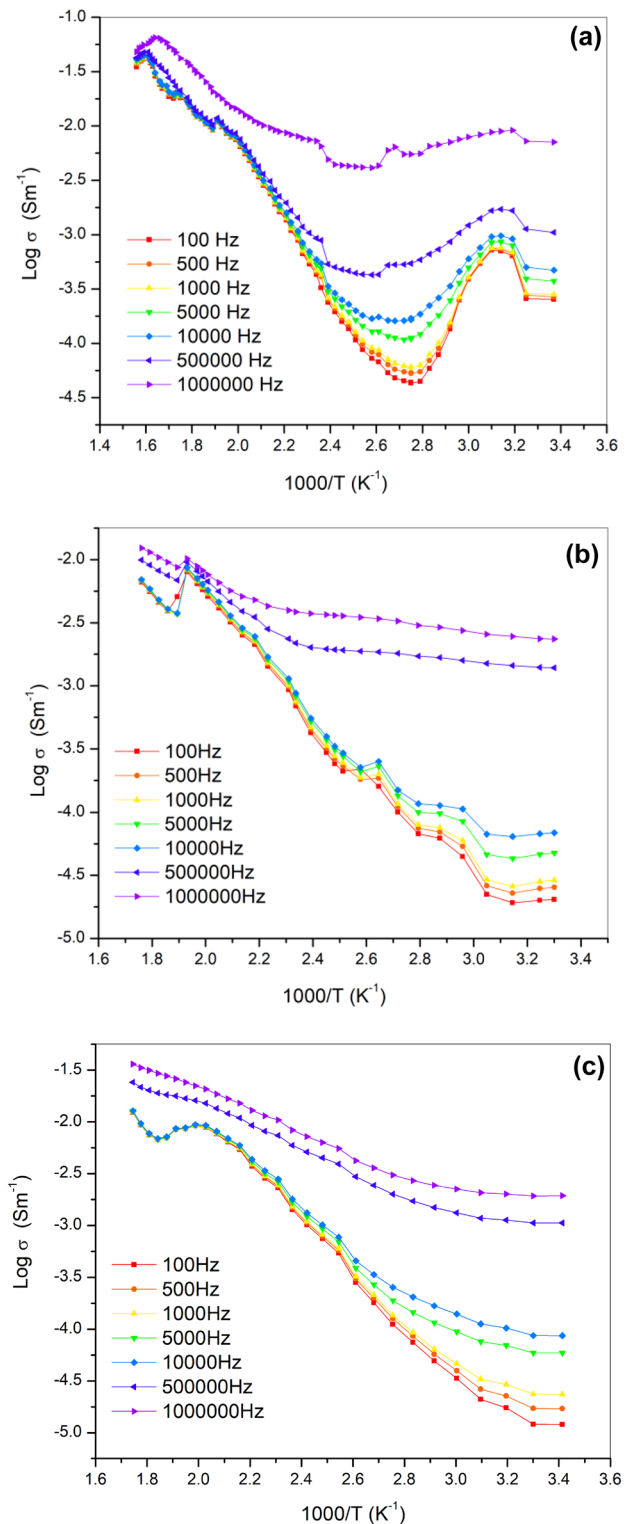


Fig. 12 Variation of logarithm A.C. conductivity with $1000/T$ at different frequencies for the heat-treated samples (1073 K) milled at different milling time **a** 5 h, **b** 10 h and **c** 50 h

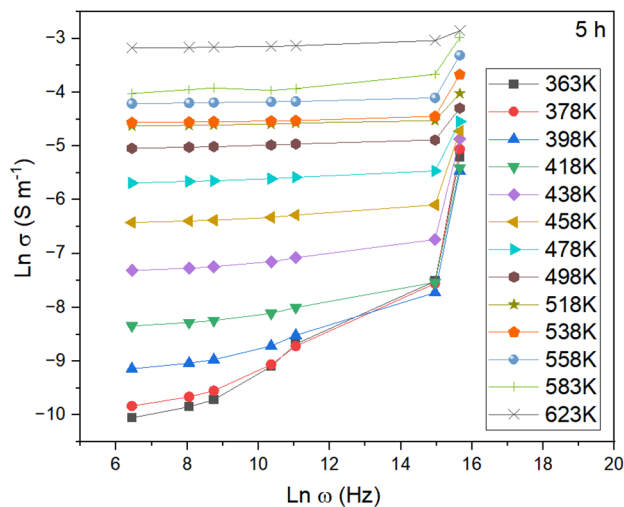


Fig. 13 Variation of $\text{Ln } \sigma$ with $\text{Ln } \omega$ at different temperature for the samples milled at 5 h

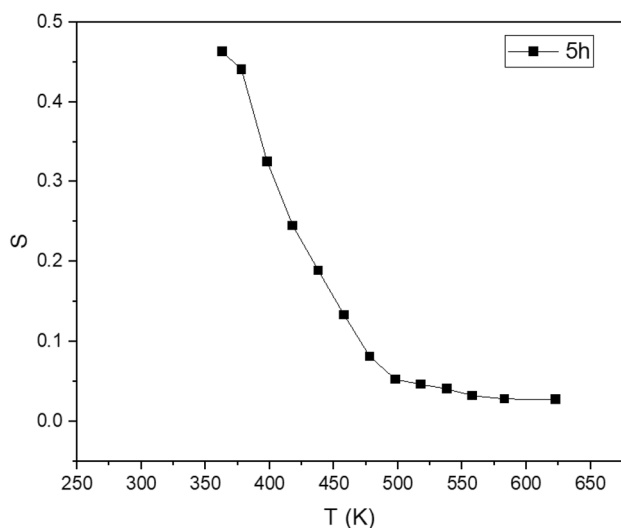


Fig. 14 Variation of exponent S with temperature for the samples milled at 5 h

formed by 88% of $\text{Bi}_2\text{Mn}_4\text{O}_{10}$ with only 5% of $\text{Bi}_{12.8}\text{O}_{19.2}$ and 7% of Mn_3O_4 is magnetically the softer one relatively to other samples and owned the minimum values of saturation magnetization (0.0842 emu/g), coercivity (41.157 G) and retentivity (0.00117 emu/g), the squareness ratio shows that the softness was decreased by increasing the milling time. All the prepared samples are electrically characterized, the peak in the dielectric constant variation with temperature is attributed to the ferroelasticity of the samples and according to Fig. 10, the ferroelectricity of the sample milled at 50 h is decreased by increasing temperature reaching the paraelectric state at 453 K which

is the same temperature of the transition peak of the temperature-dependent dielectric constant. The energy storage efficiency (η) of the sample milled at 50 h increased from 1.26% at 303 K to 98% at 453 K, accordingly, the prepared samples can be applied as energy transducer (due to their ferroelectricity) at the temperature range (450–600 K). The conduction mechanism can be described by the correlated barrier hopping (CBH). The above results leading us to try more different milling times to shift up the ferroelectric transition temperature to get an energy transducer works at high temperature.

Author contributions Study conception—SAF, MI, AEH, MMEI-D. Data collection—SAF. Analysis and interpretation of results—SAF, AEH, MMEI-D. Draft manuscript preparation—SAF, MIB, AEH, MMEI-D. All authors reviewed the results and approved the final version of the manuscript. The author confirms sole responsibility for “study conception”, “data collection”, “analysis and interpretation of results”, and “manuscript preparation”.

Funding Open access funding provided by The Science, Technology & Innovation Funding Authority (STDF) in cooperation with The Egyptian Knowledge Bank (EKB). We declare that, no funding was received for this work.

Declarations

Conflict of interest The authors declare that they have no known competing financial interests or personal relationships that could have appeared to influence the work reported in this paper.

Ethical approval We confirm that we took in consideration all the ethical rules in the this research work.

Open Access This article is licensed under a Creative Commons Attribution 4.0 International License, which permits use, sharing, adaptation, distribution and reproduction in any medium or format, as long as you give appropriate credit to the original author(s) and the source, provide a link to the Creative Commons licence, and indicate if changes were made. The images or other third party material in this article are included in the article's Creative Commons licence, unless indicated otherwise in a credit line to the material. If material is not included in the article's Creative Commons licence and your intended use is not permitted by statutory regulation or exceeds the permitted use, you will need to obtain permission directly from the copyright holder. To view a copy of this licence, visit <http://creativecommons.org/licenses/by/4.0/>.

References:

1. S.A. Fareed, M. Ibrahim, A.E. Hannora, M.M. El-Desoky, Structure, Seebeck coefficient and DC electrical conductivity of $\text{Bi}_2\text{Mn}_4\text{O}_{10}$ prepared by mechanochemical method. *J. Mater. Sci.* **33**, 15346–15358 (2022)
2. F. Ziegler, M.M. Murshed, H. Gibhardt, O. Sobolev, Th.M. Gesing, G. Eckold, Mechanical properties of multiferroic $\text{Bi}_2\text{Mn}_4\text{O}_{10}$ Full set of elastic constants determined by inelastic neutron scattering. *J. Basic Solid State Phys.* **253**, 976–982 (2016)
3. F.E.N. Ramirez, G.A. Cabrera-Pasca, J. Mestnik-Filho, A.W. Carbonari, J.A. Souza, Magnetic and transport properties assisted by

- local distortions in $\text{Bi}_2\text{Mn}_4\text{O}_{10}$ and $\text{Bi}_2\text{Fe}_4\text{O}_9$ multiferroic compounds. *J. Alloy. Compd.* **651**, 405–413 (2015)
- E. Li, H. Kakemoto, S. Wada, T. Tsurumi, Effects of manganese addition on piezoelectric properties of the (K, Na, Li) (Nb, Ta, Sb) O_3 lead-free ceramics. *J. Ceram. Soc. Jpn.* **115**, 250–253 (2007)
 - J.K. George, V.V. Halali, C.G. Sanjayan, V. Suvina, M. Sakar, R. GeethaBalakrishna, Perovskite nanomaterials as optical and electrochemical sensors. *J. Inorg. Chem. Front.* **7**, 2702–2725 (2020)
 - S. Ahmad, A. Husain, M. MujahidAliKhan, I. Khan, A. Khan, A.M. Asiri, Perovskite-based material for sensor applications. *J. Hybrid Perovskite Comp. Mater.* (2021). <https://doi.org/10.1016/B978-0-12-819977-0.00005-6>
 - G. Sun, L. Zhou, H. Sun, Y. Zhao, F. Chen, Y. Yang, Q. Zhao, Song, “ ABO_3 multiferroic perovskite materials for memristive memory and neuromorphic computing.” *Royal Soc. Chem.* **6**, 939–970 (2021)
 - M.K. Kim, J.Y. Moon, S.H. Oh, D.G. Oh, Y.J. Choi, N. Lee, Strong magnetoelectric coupling in mixed ferrimagnetic-multiferroic phases of a double perovskite. *Sci. Rep.* **9**, 5456 (2019)
 - A.K. Kundu, R. Ranjith, V. Pralong, V. Gaignaert, B. Raveau, Magneto-transport and magneto-dielectric effects in Bi-based perovskite manganites. *J. Mater. Chem.* **18**, 4280–4285 (2008)
 - J. Zhan, Y. Long, Synthesis of $\text{Bi}_2\text{Mn}_4\text{O}_{10}$ nanoparticles and its anode properties for LIB. *Ceram. Int.* **44**(12), 14891–14895 (2018)
 - Z.R. Kann, J.T. Auletta, E.W. Hearn, S.-U. Weber, K.D. Becker, H. Schneider, M.W. Lufaso, Mixed crystal formation and structural studies in the mullite-type system $\text{Bi}_2\text{Fe}_4\text{O}_9$ – $\text{Bi}_2\text{Mn}_4\text{O}_{10}$. *J. Solid State Chem.* **185**, 62–71 (2012)
 - A. Leonarska, M. KaDziołka-Gawe, A.Z. Szeremeta, R. Bujakiewicz-Koron'aska, A. Kalvane, A. Molak, Electric relaxation and $\text{Mn}^{3+}/\text{Mn}^{4+}$ charge transfer in Fe-doped $\text{Bi}_2\text{Mn}_4\text{O}_{20}$ – BiMn_2O_5 structural self-composite. *J. Mater. Sci.* **52**, 2222–2231 (2017)
 - O. De Gruyter, The crystal structures of $\text{Bi}_2\text{Mn}_4\text{O}_{10}$, $\text{Bi}_2\text{Al}_4\text{O}_9$ and $\text{Bi}_2\text{Fe}_4\text{O}_9$. *Z. Kristallogr.* **127**, 1–4 (2010)
 - Z.H. Chi, H. Yang, S.M. Feng, F.Y. Li, R.C. Yu, C.Q. Jin, Room-temperature ferroelectric polarization in multiferroic BiMnO_3 . *J. Magn. Magn. Mater.* **310**, e358–e360 (2007)
 - Z.H. Chi, C.J. Xiao, S.M. Feng, F.Y. Li, C.Q. Jin, X.H. Wang, R.Z. Chen, L.T. Li, Manifestation of ferroelectromagnetism in multiferroic BiMnO_3 . *J. Appl. Phys.* **98**(10), 103519 (2005)
 - H. Amorín, M. Venet, E. Chinarro, P. Ramos, M. Algueró, A. Castro, Lead-free $\text{Ba}_{0.85}\text{Ca}_{0.15}\text{Zr}_{0.1}\text{Ti}_{0.9}\text{O}_3$ ferroelectric ceramics with refined microstructure and high strain under electric field by mechanosynthesis. *J. Eur. Ceram. Soc.* **42**, 4907–4916 (2022)
 - R. Daly, N. Khitouni, M. Luisa Escoda, N. LlorcaIsern, S. Martínez Juan Jose, J. Marc Greneche, M. Khitouni, Microstructure, magnetic and Mössbauer studies of mechanically alloyed FeCoNi nanocrystalline powders. *Arab. J. Sci. Eng.* **46**, 5633–5643 (2021)
 - R.N. Shahid, S. Scudino, Strengthening of Al-Fe3Al composites by the generation of harmonic structures. *Sci. Rep.* **8**, 6484 (2018)
 - J.S.J. Hargreaves, Some considerations related to the use of the Scherrer equation in powder X-ray diffraction as applied to heterogeneous catalysts. *Catal. Struct. React.* **2**, 33–37 (2016)
 - T. Milenov, G. Avdeev, P. Rafailov, V. Tomov, S. Dobreva, L. Yankova, M. Veleva, D. Toncheva Growth, Characterization and dielectric properties of $\text{Bi}_2\text{Mn}_4\text{O}_{10}$ single crystals. *Comptes Rendus l'Acad. Bulg. Sci.* **64**, 931 (2011)
 - A.M. Leary, P.R. Ohodnicki, M.E. McHenry, Soft magnetic materials in high-frequency, high-power conversion applications. *JOM.* **64**, 772–781 (2012)
 - Z.S. Marinkovic, Z. Marinkovic, Z. Jaglic, M. Jagodic, L. Mancic, S. Bernik, A. Recnik, G. Brankovic, Structural and magnetic properties of nanocrystalline bismuth manganite obtained by mechanochemical synthesis. *J Nanopart Res* **13**, 3431–3439 (2011)
 - S.V. Trukhanov, I.O. Troyanchuk, V.V. Fedotova, V.A. Ryzhov, A. Maignan, D. Flahaut, H. Szymczak, R. Szymczak, Magnetic properties of the nonstoichiometric Sr-doped manganites. *Phys. Stat. Solidi. b* **242**, 1123–1131 (2005)
 - S.V. Trukhanov, Investigation of stability of ordered manganites. *J. Exp. Theor. Phys.* **101**, 513–520 (2005)
 - X. Jiang, H. Hao, Y. Yang, E. Zhou, S. Zhang, P. Wei, M. Cao, Z. Yao, H. Liu, Structure and enhanced dielectric temperature stability of BaTiO_3 -based ceramics by Ca ion B site-doping. *Journal of Materiomics.* **7**, 295–301 (2021)
 - M.M. El-Desoky, A.E. Hannora, Dielectric relaxation and impedance spectroscopy. *J Glass Phys. Chem.* **46**, 487–496 (2020)
 - M. Coşkun, Ö. Polat, F.M. Coşkun, Z. Durmuş, M. Çağlar, A. Türüt, The electrical modulus and other dielectric properties by the impedance spectroscopy of LaCrO_3 and $\text{LaCr}_{0.90}\text{Ir}_{0.10}\text{O}_3$ perovskites. *RSC. Adv.* **8**, 4634–4648 (2018)
 - M. Rekaby, Dielectric response and cole-cole plot analysis for $(\text{Zn}_{0.91}\text{Mn}_{0.03}\text{CO}_{0.06}\text{O})\text{X}/\text{Cu}_{0.5}\text{Ti}_{0.5}\text{Ba}_2\text{Ca}_2\text{Cu}_3\text{O}_{10-\delta}$ diluted magnetic semiconductor/superconductor composites. *J. Appl. Phys. A.* **126**, 1–9 (2020)
 - B.M. Greenhoe, M.K. Hassan, J.S. Wiggins, “Universal power law behavior of the AC conductivity versus frequency of agglomerate morphologies in conductive carbon nanotube-reinforced epoxy networks.” *J. Polym. Sci Part B: Polym. Phys.* **54**, 1918–1923 (2016)
 - V. Thakur, A. Singh, A.M. Washi, L. Singh, Temperature dependent electrical transport characteristics of BaTiO_3 modified lithium borate glasses. *AIP Adv.* **5**, 087110 (2015)
 - A. Ghosh, Frequency-dependent conductivity in bismuth-vanadate glassy semiconductors. *Phys. Rev. B* **41**, 1479 (1990)
 - R. Long, Frequency-dependent loss in amorphous semiconductors. *Adv. Phys.* **31**, 553 (1982)

Publisher's Note Springer Nature remains neutral with regard to jurisdictional claims in published maps and institutional affiliations.